# Anisotropic Superconductivity in Layer Compounds*†

R. C. Morris and R. V. Coleman
*Department of Physics, University of Virginia, Charlottesville, Virginia 22901*
(Received 14 August 1972)

Measurements of the angular dependence of the upper critical field $H_{c2}$ in the transition metal dichalcogenides $TaS_2$, $TaS_2$-(pyridine), $TaS_1Se_1$, $TaS_1Se_1$-(pyridine), $TaS_{1.2}Se_{0.8}$, and $TaS_{0.8}Se_{1.2}$ have been made in magnetic fields up to 150 kOe. The observed angular dependence has been compared to simple theoretical models in order to estimate the anisotropy of the coherence length $\xi$ in these materials. The values of the $\xi_\parallel/\xi_\perp$ calculated from the data were 20 for $TaS_2$-(pyridine) and approximately 7 for the $TaS_2$, $TaS_1Se_1$, and $TaS_1Se_1$-(pyridine). The alloys with different ratios of sulfur and selenium showed no major change in behavior as compared to $TaS_1Se_1$. The results are also discussed in relation to a generalized effective-mass model of anisotropic electronic conduction. The resistive transitions in the intercalated materials for field orientations less than 10° from the parallel orientation are extremely broad and also exhibit unusual structure connected with enhanced flux-flow resistance. The magnetoresistance behavior in the normal state of the pure and intercalated layer compounds has also been measured and the changes in anisotropy due to intercalation are discussed.

## I. INTRODUCTION

Transition-metal dichalcogenides formed from the 5*d* transition-metal series contain a number of layered structures which exhibit a superconducting phase transition. Superconducting properties of these materials such as critical field, critical current, and magnetization all show a high degree of anisotropy, and data on these anisotropies have been reported by a number of authors.[1-3] In addition, several of these compounds can be intercalated by diffusing an organic material into the van der Waals gap between the layers. Such intercalation substantially increases the distance between the successive layers of metal atoms, and large increases in the anisotropy of the electronic properties are observed upon intercalation.[4]

A convenient method for studying the superconducting anisotropy in both the pure and intercalated materials consists of measuring the resistive transition which occurs as a magnetic field is applied to the specimen. This method allows one to make a reasonably accurate measurement of the critical field as a function of angle and such measurements on pure $NbSe_2$ have been reported by us in a previous paper.[5]

In the present paper we report similar measurements on a number of layer structures including several intercalated with pyridine ($C_6H_5N$).

## II. EXPERIMENTAL PROCEDURE

The dichalcogenide compounds were fabricated by heating stochiometric amounts of the appropriate elements in sealed quartz tubes to a temperature of 600 °C in the case of $NbSe_2$ and 925 °C for all of the tantalum compounds. Starting materials of purity 99.9% or better were used. Crystals of $NbSe_2$, $TaS_2$, $TaS_1Se_1$, $TaS_{1.2}Se_{0.8}$, and $TaS_{0.8}Se_{1.2}$ were prepared by the method of iodine-transport reaction according to well-established procedures.[6] All crystals grew in platelet geometry. The preparation and characteristics of the $NbSe_2$ crystals have been previously described.[5] The $TaS_2$ crystals were probably less perfect than those of $NbSe_2$, since the surfaces were rather wrinkled in appearance in contrast to shiny mirrorlike surfaces observed on the $NbSe_2$ crystals. The $TaS_xSe_y$ crystals were apparently of somewhat better quality since they had fairly smooth surfaces. Samples were prepared by slicing the crystals into bar-shaped samples with widths of 0.2 – 0.5 mm and lengths of 2 – 6 mm. The thickness perpendicular to the layers was in the range 0.05 – 0.3 mm. Electrical connections were made using lead-tin solder and conducting paint. Resistance measurements were made using a standard four-lead arrangement.

Intercalated samples of $TaS_2$ and $TaS_1Se_1$ were prepared by first cutting the crystals to the desired sample dimensions and then heating in an excess of pyridine. A temperature of 200 °C was used for the intercalation of $TaS_2$, while intercalation of $TaS_1Se_1$ required temperatures of around 300 °C. The crystals of $TaS_2$-(pyridine) which were measured in the present experiments showed expansions of about 98% in the *c*-axis direction upon intercalation, and this is in good agreement with other reported experiments.[7] However, there were some crystals which showed less expansion in the range down to 70%. These crystals tended to have lower and more smeared temperature transitions as well as electrical behavior which deviated from the more perfectly intercalated crystals.

The $TaS_1Se_1$ showed a considerable variation in the expansion occurring upon intercalation with values ranging from 30 to 140%. No direct correla-

tion was made between the electrical properties and the amount of expansion, but the experiments indicated that a larger expansion produced a lower transition temperature.

For the $TaS_xSe_y$ crystals the $a$-axis resistivities at 4.2 °K were all around $5 \times 10^{-5}$ Ω cm. For the $TaS_2$ and $TaS_2$-(pyridine) crystals used in the experiments the $a$-axis resistivities at 4.2 °K were both on the order of $10^{-5}$ Ω cm, in good agreement with previously reported values.[4] In a few cases the intercalated $TaS_2$ crystals showed considerably higher calculated resistivities which we associate with conduction by only a fraction of the layers due either to crystal imperfection or imperfect current contacts. Current densities were kept relatively low for most measurements and were on the order of 10 A/cm$^2$.

The experiments were performed by rotating the samples in magnetic fields generated by superconducting solenoids for fields up to 80 kOe and by Bitter solenoids for fields up to 150 kOe. The samples were mounted with the current always transverse to the magnetic field and the rotating sample holders used were capable of an angular alignment to an accuracy of ± 0.1 °.

## III. EXPERIMENTAL RESULTS

### A. $TaS_2$ and $TaS_2$-(Pyridine)

The perfect as-grown form of 2$H$-$TaS_2$ has a superconducting transition temperature of 0.8 °K, and magnetic field experiments in the superconducting phase have not yet been carried out in detail. However, in this paper we do report data on one specimen of $TaS_2$ with a $T_c$ above 1 °K. As originally reported by Gamble *et al.*,[7] the transition temperature of $TaS_2$ can be raised to approximately 3.5 °K by intercalation with pyridine.

Intercalation with pyridine changes the spacing between the layers of tantalum atoms from 6 Å to approximately 12 Å as reported in Refs. 4 and 7. The resistivity in the $c$-axis direction increases by as much as four orders of magnitude upon intercalation[4] while the resistivity parallel to the layers increases only slightly. This behavior is consistent with the idea that the intercalated material should show physical properties approaching those of a two-dimensional conductor. With this idea in mind we have examined the resistive transition induced by magnetic fields up to 150 kOe. We have also studied the resistive transition occurring as the current is increased to the critical current for various values of the magnetic field applied parallel and perpendicular to the layers.

We have made detailed measurements of the field-induced resistive transition in $TaS_2$-(pyridine) for five separate specimens and the exact shape and width of the transition appears to be quite specimen dependent. This behavior suggests a strong correlation with the perfection and uniformity of the intercalated layers, and this is particularly evident for transitions observed at field orientations less than 10 ° from the direction parallel to the layers. For these field orientations the resistive transition becomes very broad and the resistance rises very slowly toward the normal-state resistance as the field is increased. In addition, structure in the resistive transition which appears to be connected with flux flow becomes pronounced at the lower angular orientations of the field. The flux-flow structure is, in fact, so broad that it is difficult to select a unique value of $H_{c2}$ at the lower angles. For the parallel field orientation, $H_{c2}$ is greater than the maximum field of 150 kOe used in the experiments. The general behaviors of the field-induced resistive transition, the width of the superconducting transition as a function of temperature, and the magnetoresistance rotation curves appear to allow a selection of the crystals on the basis of perfection and we therefore present data that we estimate to be characteristic of the more perfect $TaS_2$-(pyridine) crystals. A typical curve of resistance as a function of temperature at $H = 0$ for a more perfect intercalated crystal is shown in Fig. 1(a). This crystal had an initial resistivity parallel to the layers at 4.2 °K of $\rho_a = 1 \times 10^{-5}$ Ω cm. After a number of experiments and cycling from room temperature to helium temperature, the resistivity was remeasured and had increased to $\rho_a = 6 \times 10^{-5}$ Ω cm at 4.2 °K. These resistivities compare quite well with the value of $\rho_a = 6 \times 10^{-5}$ Ω cm measured at 4.2 °K by Thompson *et al.*[4] for $TaS_2$-(pyridine).

Figure 1(b) shows data on the field-induced resistive transition at 1.4 °K measured in fields up to 150 kOe. For this temperature the parallel orientation of the field shows no resistance induced up to 150 kOe even from flux flow. There is, however, marked flux flow at higher angles which produces broad maxima and minima at angles between 1 ° and 10 ° from the parallel orientation. At higher temperatures approaching $T_c$ this flux-flow structure becomes more pronounced and resistance transitions measured at 2.8 °K are shown in Figs. 2(a) and 2(b).

The two sets of curves show positive and negative angles measured on either side of the parallel orientation. The asymmetry of the flux-flow resistivity between these two equivalent orientations suggests that the resistive structure is connected with a specific crystal defect. The positive angles of Fig. 2(a) correspond to the same positive angles measured in Fig. 1(b) at the lower temperature. An interesting behavior at the higher temperature is observed for the 4 ° orientation where the maximum resistance rises considerably above the nor-

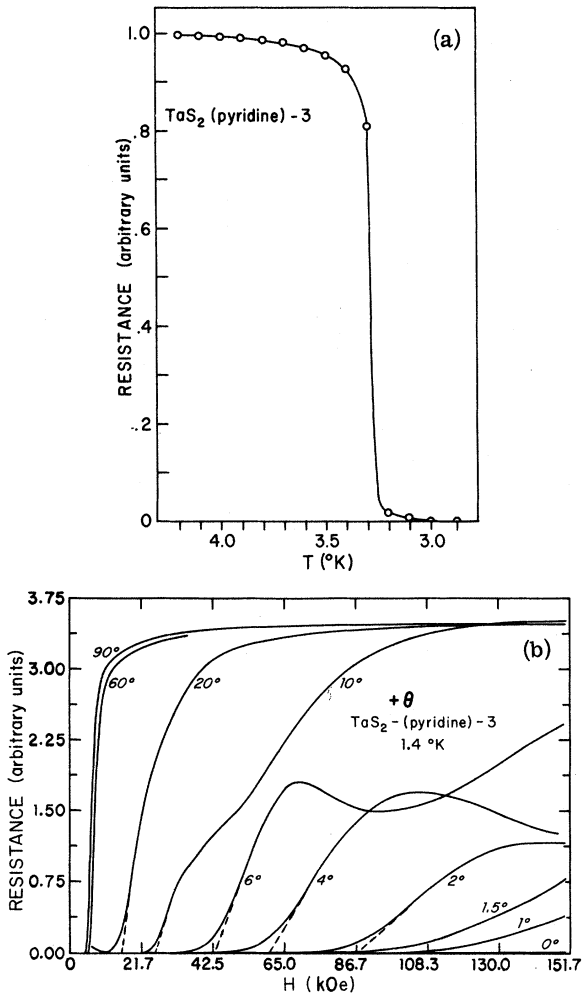


FIG. 1. (a) Resistance vs temperature for $TaS_2$-(pyridine) sample around $T_c$. (b) Resistance transition in a magnetic field. Angles refer to field directions relative to the plane of the layers of the crystal.

mal resistance. A resistance maximum followed by a resistance minimum is the type of structure seen in other type-II superconductors and is often referred to as the "peak effect." However, the present structure is very broad and not characterized by an abrupt rise of resistance after the minimum as is usually observed in the "peak effect."[8]

The magnetoresistance rotation curves observed for this sample at temperatures of 1.5 and 2.8 °K correlate with the field-sweep curves just described and are shown in Figs. 3(a) and 3(b). These again show the maximum-minimum resistance structure at the appropriate angles and also show the same increase in magnitude at the higher temperature. For fields at angles greater than 10° from the parallel orientation the transitions are smooth and occur over a fairly narrow field range with the resistance reaching a uniform normal value. In this respect the transitions above 10° are similar to the behavior in the unintercalated layer structures and allow a reasonably consistent interpretation of $H_{c2}$ from the construction indicated by the dotted line in Fig. 1(b).

One of the as-grown $TaS_2$ crystals measured was entirely superconducting at temperatures below 1.1 °K. The angular dependence of the critical field was measured for this crystal at 1.03 °K and the resistive transitions for all angles were smooth and typical of the other as-grown layer compounds. The higher transition temperature of this particular sample may be associated with the presence of additional phases quenched in upon cooling from high temperature, and this may also account for the 2 °K width of the temperature transition in zero field. Although this crystal may not be typical of a more perfect $TaS_2$ crystal, the data are interesting for comparison to the data on intercalated

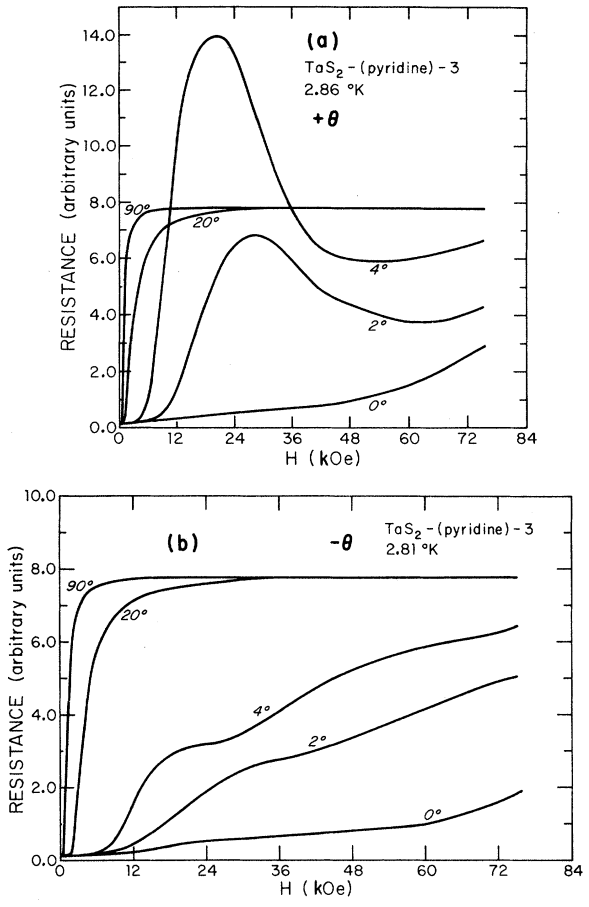


FIG. 2. Resistance transition in a magnetic field for $TaS_2$-(pyridine). Parts (a) and (b) show behavior for positive and negative angles of the field measured on either side of the field orientation parallel to the layers. Part (a) corresponds to same field orientations shown in Fig. 1(b).

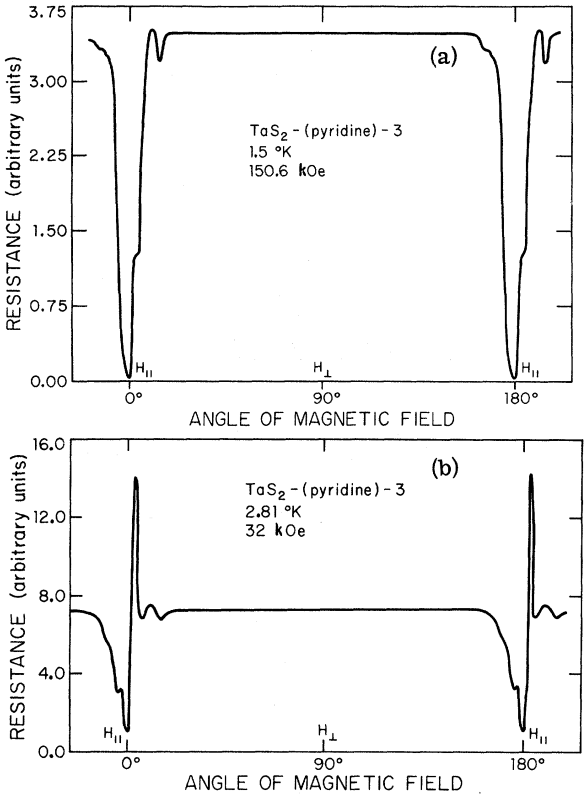


FIG. 3. Resistance vs angle of magnetic field with plane of the layers for $TaS_2$-(pyridine) at two different temperatures, fields, and current densities.

$TaS_2$, and this comparison is made in Fig. 10(a).

In the case of $TaS_2$ and $TaS_2$-(pyridine) we have also measured the magnetoresistance behavior at 4.2 °K where both specimens are in the normal state, and data on field dependence and magnetoresistance anisotropy are shown in Fig. 4. Both the anisotropy of the rotation diagrams and the field dependence of magnetoresistance show a marked difference between the as-grown specimen and the intercalated specimen. The as-grown specimen shows a monotonically increasing magnetoresistance for both the $H_\parallel$ and $H_\perp$ orientations and the rotation curve shows a broad smooth anisotropy. Both of these features are generally characteristic of an anisotropic three-dimensional metal. On the other hand, the intercalated specimen shows an unusual negative magnetoresistance for the $H_\perp$ orientation and much sharper anisotropy in the rotation curve near the $H_\parallel$ orientation. This major change in the normal-state magnetoresistance observed upon intercalation may be evidence that the electrons are being more closely confined within the individual layers than for the as-grown material, since limitation of the mean free path along the $c$ axis could be responsible for such a change. This normal-state magnetoresistance behavior is typical of all of the intercalated specimens measured.

The current-induced resistance transitions for a $TaS_2$-(pyridine) crystal are represented by the

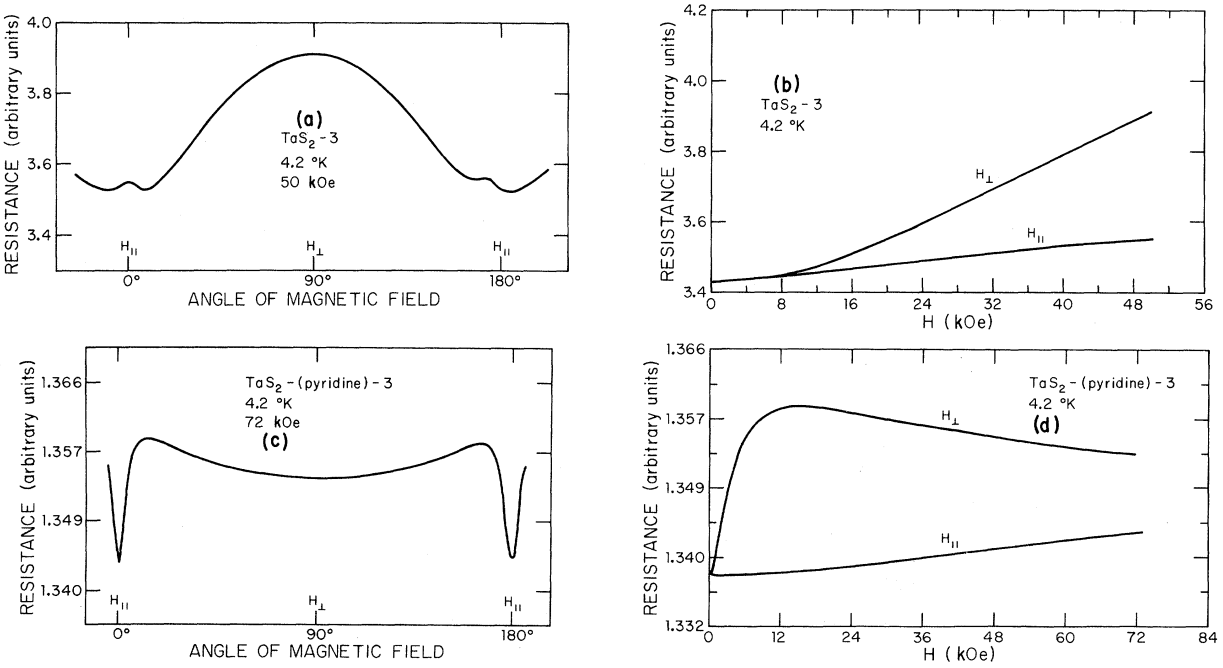


FIG. 4. Resistance as a function of applied magnetic field for $TaS_2$ and $TaS_2$-(pyridine) samples when both are in the normal state at 4.2 °K. Parts (a) and (c) show resistance vs angle of magnetic field for the two samples. Parts (b) and (d) show resistance vs magnetic field for field directions parallel and perpendicular to the layers.

current-voltage curves shown in Fig. 5 for increasing values of the magnetic field parallel to the layers. At zero magnetic field the voltage rises very slowly as the current is increased up to the critical value and then jumps abruptly to approximately the voltage corresponding to the normal-state resistance as represented by the Ohmic $I$-$V$ curve obtained in a perpendicular field of 4 kOe. The current-voltage transitions for intermediate-field values parallel to the layers show a more rapid increase in resistance and successively smaller discontinuous voltage jumps as the field is increased. The increased resistance observed before the abrupt transition to the normal state suggests a resistance contribution from flux flow, although the current and field dependence do not seem to follow the usual models.

### B. $TaS_1Se_1$, $TaS_{1.2}Se_{0.8}$, $TaS_{0.8}Se_{1.2}$, and $TaS_1Se_1$-(Pyridine)

We have also examined several alloys composed of tantalum, sulfur, and selenium since these have transition temperatures considerably above 1 °K for the as-grown materials. For the specimens reported here the transition temperatures were $TaS_1Se_1$, 3.7 °K; $TaS_{1.2}Se_{0.8}$, 3.9 °K; and $TaS_{0.8}Se_{1.2}$, 3.9 °K. The behavior of the critical field and the magnetoresistance were essentially the same for all three alloys so we will present principally the data on $TaS_1Se_1$ as representative. The resistance transitions induced by the magnetic field for various angles between the magnetic field and the layers are shown in Fig. 6(a). For the as-grown $TaS_1Se_1$ these are smooth and fairly sharp even at the lowest angles. The behavior is quite similar to that observed in the layer structure $NbSe_2$ previously reported.[5] The critical fields for the field orientations parallel and perpendicular to the layers are linear functions of the temperature below $T_c$ as shown in Fig. 7. This is similar

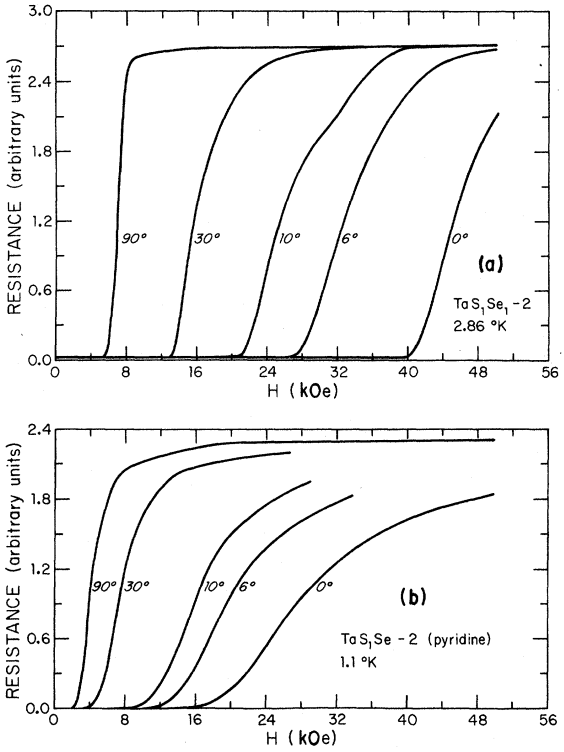


FIG. 6. Resistance transition in a magnetic field for $TaS_1Se_1$ and $TaS_1Se_1$-(pyridine) samples. Angles refer to field directions relative to the plane of the layers of the crystals.

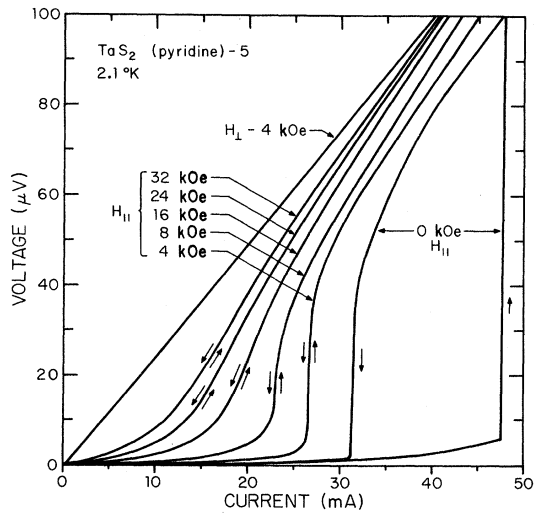


FIG. 5. $I$-$V$ curves for superconducting $TaS_2$-(pyridine) for different applied magnetic fields parallel to layers. Ohmic curve is for perpendicular field such that sample is in the normal state.

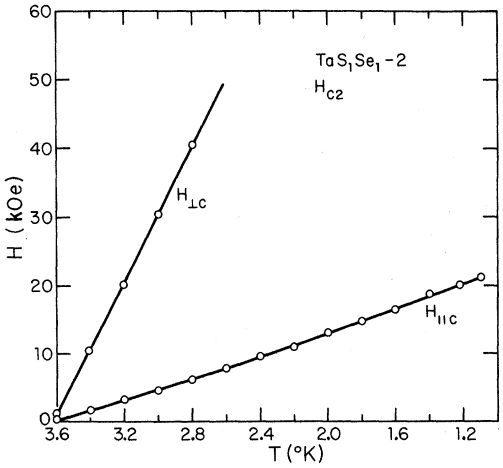


FIG. 7. $H_{c2}$ for $TaS_1Se_1$ as a function of temperatures for fields parallel and perpendicular to the layers.

to the behavior reported for other superconducting layer compounds.[9]

The $TaS_1Se_1$ specimens were also intercalated with pyridine and the resistive transition as a function of field angle was again measured. The results are shown in Fig. 6(b) and indicate a much broader resistive transition in the intercalated material particularly at lower angles. The transition temperature $T_c$ was lowered from 3.7 to 1.5 °K upon intercalation and indicates that a fairly large change in the electron-phonon interaction has taken place. The critical field ratio versus angle for all of the compounds $TaS_1Se_1$, $TaS_1Se_1$-(pyridine), $TaS_{0.8}Se_{1.2}$, and $TaS_{1.2}Se_{0.8}$ shows a similar behavior, and examples are plotted in Fig. 8 and give a value of $(H_{c2\parallel}/H_{c2\perp})^2$ of between 40 and 50 for all of the specimens measured. The normal-state magnetoresistance curves taken at 4.2 °K for both the as-grown and pyridine-intercalated $TaS_1Se_1$ are shown in Fig. 9 and indicate a similar anisotropy in both cases, in contrast to the $TaS_2$ case where the intercalation had a marked effect on the anisotropy of the normal-state magnetoresistance. The critical-field data for all of the specimens measured in the present experiments are summarized in Table I along with data on the critical temperature $T_c$ and the reduced temperature $t = T/T_c$ corresponding to the critical-field measurement.

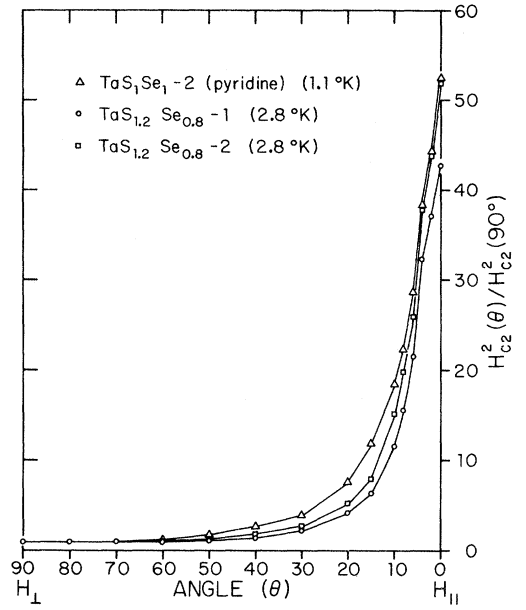


FIG. 8. Experimental curve of $H_{c2}^2(\theta)/H_{c2}^2(90°)$ vs angle of magnetic field with plane of layers for $TaS_{1.2}S_{0.8}$ and $TaS_1Se_1$-(pyridine) samples.

## IV. DISCUSSION

### A. Elliptical-Fluxoid Model

In the case of a layered superconductor, one of the simplest models which can be used to explain the anisotropy observed for the upper critical field is to assume an elliptical fluxoid and to use the straightforward result of Ginsburg–Landau theory[10] for type-II superconductors which relates $H_{c2}$ to the fluxoid through the following expression:

$$H_{c2} = \phi_0/2\pi\xi_a\,\xi_b\,, \qquad (1)$$

where $\phi_0$ is the flux quantum and $\xi_a$ and $\xi_b$ are the two principal coherence lengths in the plane perpendicular to $H$.

The model assumes that $\xi$ is isotropic within the layers and is described by an ellipsoidal surface for other directions.[5] The generalized coherence length is then represented by the tensor

$$\begin{pmatrix} \xi & 0 & 0 \\ 0 & \xi & 0 \\ 0 & 0 & \epsilon\xi \end{pmatrix},$$

where $\xi_\perp = \epsilon\xi_a = \epsilon\xi$. For $H$ perpendicular to the layers the fluxoid is therefore circular in cross

TABLE I. Summary of critical-field data for specimens measured in present experiments as well as data on the critical temperature $T_c$ and reduced temperature $t$ corresponding to critical-field measurements.

| | $T_c$ (°K) | $T$ (°K) | $t$ | $H_{c2\perp}$ (kOe) | $H_{c2\parallel}$ (kOe) | $H_{c2\perp}/T_c$ (kOe/°K) | $(H_{c2\parallel}/H_{c2\perp})^2$ |
|---|---|---|---|---|---|---|---|
| $NbSe_2$-2 | 7.0 | 4.2 | 0.60 | 22.1 | 74.1 | 3.16 | 11.2 |
| $NbSe_2$-5 | 7.0 | 4.2 | 0.60 | 19.5 | 71.4 | 2.79 | 13.4 |
| $TaS_1Se_1$-1 | 3.7 | 2.2 | 0.60 | 9.0 | 53.9 | 2.43 | 35.9 |
| $TaS_1Se_1$-2 | 3.7 | 2.2 | 0.60 | 11.0 | 73.8 | 2.96 | 45.2 |
| $TaS_{1.2}Se_{0.8}$-1 | 3.9 | 2.34 | 0.60 | 11.5 | 75.2 | 2.96 | 42.8 |
| $TaS_{1.2}Se_{0.8}$-2 | 3.9 | 2.34 | 0.60 | 12.8 | 92.1 | 3.28 | 51.8 |
| $TaS_{0.8}Se_{1.2}$-1 | 3.9 | 2.9 | 0.74 | 6.7 | 45.0 | | 45.4 |
| | | 2.34 | 0.60 | 10.4 | | 2.67 | |
| $TaS_1Se_1$(pyridine)-2 | 1.5 | 1.1 | 0.73 | 2.6 | 19.1 | | 52.4 |
| | | 0.9 | 0.60 | 4.0 | | 2.64 | |
| $TaS_2$(pyridine)-3 | 3.25 | 2.0 | 0.61 | 1.4 | >66 | 0.42 | >2000 |
| | | 1.4 | 0.43 | 4.9 | >150 | | >940 |

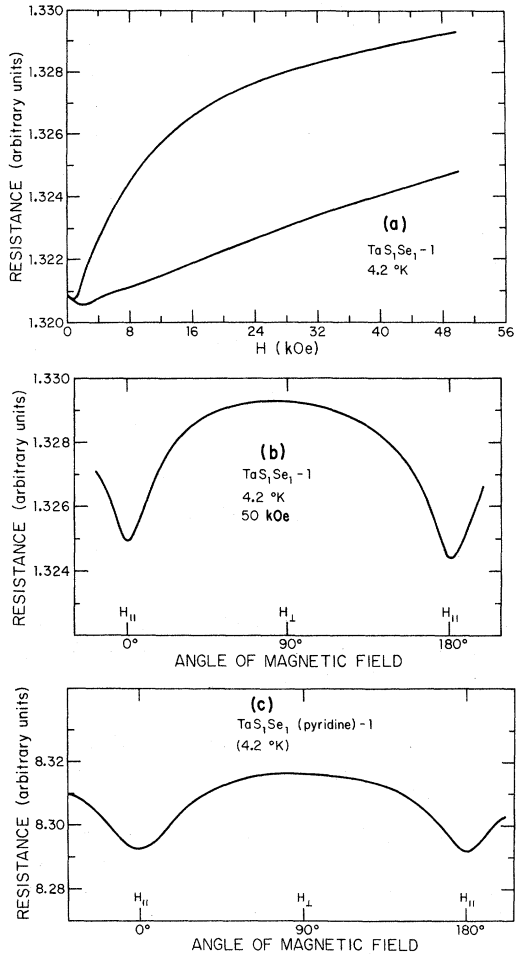


FIG. 9. Magnetoresistance of $TaS_1Se_1$ and $TaS_1Se_1$-(pyridine) when both are in the normal state above $T_c$. Part (a) shows resistance vs magnetic field for orientations parallel and perpendicular to the layers in $TaS_1Se_1$. Parts (b) and (c) show resistance as a function of angle of magnetic field at 50 kOe.

section, while for other field directions it is elliptical in cross section with the greatest ratio $\xi_a/\xi_b = \xi/\epsilon\xi = \xi_\parallel/\xi_\perp$ obtained for $H$ parallel to the layers. The ellipsoidal model with $H_{c2}$ given by (1) results in the following expressions for the angular dependence[5] of $H_{c2}$:

$$H_{c2}(\theta) = \frac{\phi_0}{2\pi\xi^2(\sin^2\theta + \epsilon^2\cos^2\theta)^{1/2}} \tag{2}$$

or

$$\frac{H_{c2}^2(\theta)}{H_{c2}^2(90°)} = \frac{1}{\sin^2\theta + \epsilon^2\cos^2\theta}\,, \tag{3}$$

where $\theta$ is the angle between $H$ and the layers. The physical idea expressed by Eqs. (1) and (2) is that the superconductivity is destroyed when the hard cores of the fluxoids begin to overlap and that the elliptical variation of the fluxoid cross section allows for a higher packing density of hard cores at lower angles and consequently higher critical fields as expressed by Eq. (2).

The upper critical field of course depends on the details of the fluxoid packing and on the complete structure of the fluxoid. The accuracy of the above simplified model may therefore vary from material to material and may depend on the anisotropy and how it affects the detailed structure of the fluxoid. In particular, when the coherence length perpendicular to the layers is on the order of the layer spacing, the validity of the model may be questionable.

### B. Effective-Mass Model

Various theoretical models of superconducting layer structures have introduced the idea of an effective mass to describe the electron conduction parallel and perpendicular to the layers. In such models the effective mass can be represented by a tensor of the form

$$\begin{pmatrix} m_\parallel & 0 & 0 \\ 0 & m_\parallel & 0 \\ 0 & 0 & m_\perp \end{pmatrix},$$

and the coherence length in the direction perpendicular to the layers is then related to the coherence length in the plane of the layers by

$$\xi_\perp = (m_\parallel/m_\perp)^{1/2}\,\xi_\parallel\,. \tag{4}$$

Lawrence and Doniach[11] have developed such a model based on the idea that the superconducting order parameter in adjacent layers is coupled by Josephson tunneling and that the $z$ dependence of single-particle states is described by a tight-binding form. The highly anisotropic effective mass represented in this case is a generalized one and can include contributions from the band effective-mass anisotropy as well as anisotropy in the electron-phonon interaction.

The critical-field experiments described in the present paper can be fitted to Eq. (3) in order to determine a value of $\epsilon^2$. The generalized effective-mass ratio can then be determined from the relation

$$\epsilon^2 = \frac{m_\parallel}{m_\perp} = \frac{\xi_\perp^2}{\xi_\parallel^2}\,. \tag{5}$$

### C. Critical Fields in $NbSe_2$

Data on the angular dependence of the upper critical field measured in pure single crystals of $NbSe_2$ were compared to the model represented by Eq. (3) and details have been reported in Ref. 5. The model gave a reasonably good fit to the data and the best value of the adjustable parameter $\epsilon^2$ was determined to be $0.09 \pm 0.01$. Using $1/\epsilon = \xi_\parallel/\xi_\perp$

we therefore obtain an estimate of 3.3 for the ratio $\xi_{\parallel}/\xi_{\perp}$ in $NbSe_2$. The effective-mass ratio calculated from Eq. (5) gives $m_{\perp} \approx 11 m_{\parallel}$, as reported in Ref. 5.

In the case of $NbSe_2$, Bachmann *et al.*[12] have used optical-absorption measurements at 2 °K to determine the plasma frequency and can therefore determine the bare electron mass from the expression $\omega_p^2 = 4\pi ne^2/m^*$. They obtain a value of $m^* = 9.7 m_e$, where $m_e$ is the free-electron mass. These authors also estimate the value of the electron-phonon coupling constant $\lambda$ in $NbSe_2$ by using the relation $m_{th} = m^*(1+\lambda)$ and adjusting $\lambda$ to give the thermal-mass value determined from specific-heat measurements.[13] The estimated value was $\lambda = 0.36$ which is the range of a BCS-type superconductor. These estimates could not take into account any anisotropic effects, but the plasma edge determined in the optical experiment might be expected to be more characteristic of electronic response in the plane of the layers. The estimate of $m_{\perp} = 11 m_{\parallel}$ would therefore indicate a very large effective mass for conduction perpendicular to the layers in $NbSe_2$, although an exact value cannot be estimated until more is known about the anisotropy in the electron-phonon interaction.

### D. Critical Fields in $TaS_2$ and $TaS_2$-(Pyridine)

As pointed out previously, the pure perfect $TaS_2$ crystals have a $T_c$ of 0.8 °K while some of the crystals with either imperfections or slight phase admixtures have a $T_c$ above 1 °K. Critical-field data for one of the crystals with a high $T_c$ are shown by the triangular points in Fig. 10(a). The dashed curve indicates the theoretical curve calculated from Eq. (3) with a value of $\epsilon^2 = 0.022$. The approximate coherence-length ratio is therefore given by $\xi_{\parallel}/\xi_{\perp} = 1/\epsilon = \sqrt{45} \sim 6.7$, while the effective-mass ratio $m_{\perp}/m_{\parallel} = 1/\epsilon^2$ gives $m_{\perp} = 45 m_{\parallel}$.

The angular dependence of the critical-field ratio $H_{c2}^2(\theta)/H_{c2}^2(90°)$ for $TaS_2$-(pyridine) is also plotted in Fig. 10(a). The dashed lines again show the values of $H_{c2}^2(\theta)/H_{c2}^2(90°)$ calculated from Eq. (3). The data follow a $1/\sin^2\theta$ dependence for most of the angular range. Deviations occur for values of $\theta$ less than 10° and data for these angles are replotted on an expanded scale in Fig. 10(b). The values of the ratio $H_{c2}^2(\theta)/H_{c2}^2(90°)$ measured from the resistance transitions at 2.86 °K show a small deviation from $1/\sin^2\theta$ below 3°, while the data measured at 1.4 °K deviate from $1/\sin^2\theta$ below 10° as shown. The 1.4 °K data fit fairly well to the values calculated from Eq. (3) with $\epsilon^2 = 0.00242$ or $1/\epsilon^2 = 413$ as indicated by the dashed curve so labeled in Fig. 10(b). In terms of the coherence lengths this number gives a ratio $\xi_{\parallel}/\xi_{\perp} = \sqrt{413} \approx 20$ while the effective-mass relation gives $m_{\perp} \approx 400 m_{\parallel}$. The values of $H_{c2}$ used for the above model comparison were calculated using the construction shown by the dotted extrapolation indicated in Fig. 1(b).

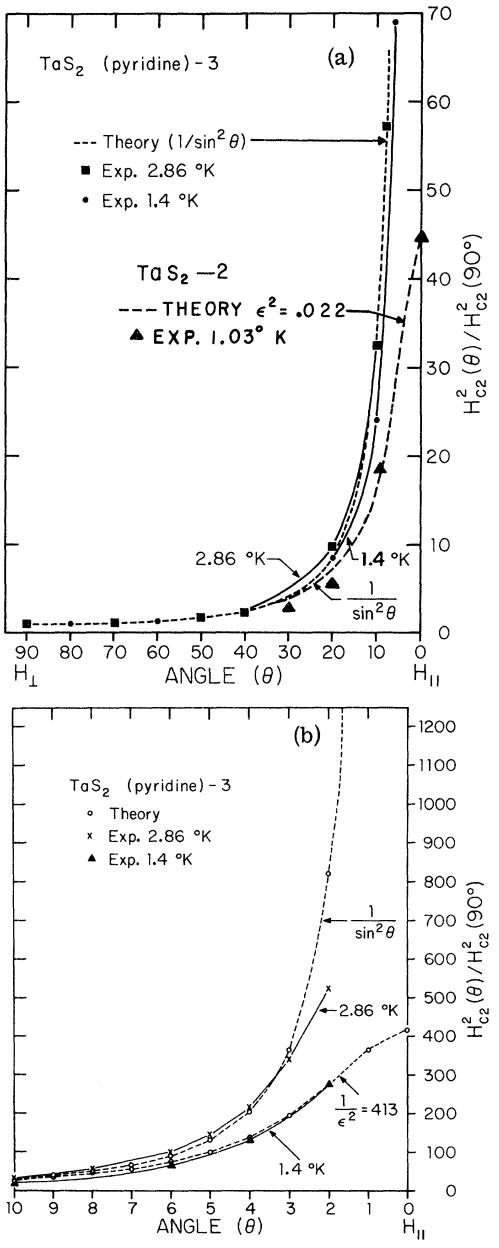


FIG. 10. $H_{c2}^2(\theta)/H_{c2}^2(90°)$ vs angle $\theta$ of the magnetic field with plane of the layers for $TaS_2$-(pyridine) sample and $TaS_2$ crystal. Part (a) shows entire angular range and dotted lines show curves of $1/\sin^2\theta$ and $1/(\sin^2\theta + \epsilon^2 \times \cos^2\theta)$ with $\epsilon^2 = 0.022$. (b) Data on $TaS_2$-(pyridine) for angular range below 10°. Curves for $1/\sin^2\theta$ and $1/(\sin^2\theta + \epsilon^2 \cos^2\theta)$ with $\epsilon^2 = 0.0024$ are shown for comparison.

The reason for the difference in the behavior of the critical-field ratios below $\theta = 10°$ for the two temperatures just discussed is not certain at pres-

ent. One possibility is that the flux-flow resistance structure is considerably different at the two temperatures and introduces differences in the construction used to obtain $H_{c2}$, particularly below angles of 10°. The temperature modification of the flux flow is clearly evident for the 4° orientation where the resistance maximum observed moves down in field by as much as 80 kOe as the temperature is raised from 1.4 to 2.8 °K. The construction for $H_{c2}$ used here represents a minimum value for $H_{c2}$ at low angles since it assigns most of the apparent flux-flow resistance structure to fields greater than $H_{c2}$. On the other hand, if larger values of $H_{c2}$ are picked at low angles, one must conclude that $H_{c2}$ rises much faster than $1/\sin^2\theta$ at low angles since the high-angle transitions are too narrow to allow sufficient upward adjustment of $H_{c2}$ in order to maintain the $1/\sin^2\theta$ dependence. The resolution of this point will have to await a more exact understanding of the resistance structure at low angles as well as a more refined model of the critical-field behavior expected near the parallel orientation of the field.

### E. Critical Fields in $TaS_1Se_1$ and $TaS_1Se_1$-(Pyridine)

The critical-field data on $TaS_1Se_1$ are represented by the solid circles in Fig. 11. The best fit of the function in Eq. (3) is represented by the open circles and gives a value of $\epsilon^2 = 0.022$. This is the same value as determined for the pure $TaS_2$ and gives an approximate coherence-length ratio of

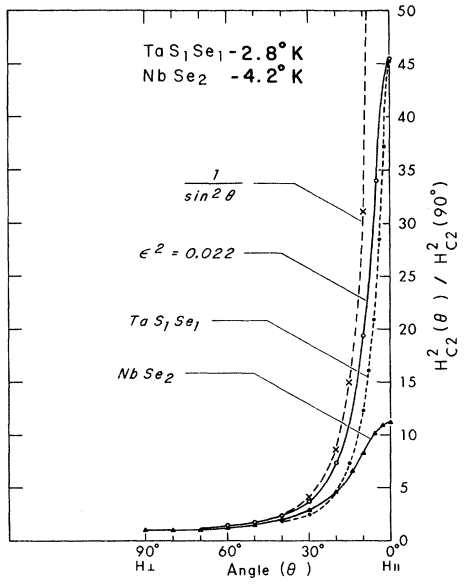


FIG. 11. Experimental curve of $H_{c2}^2(\theta)/H_{c2}^2(90°)$ vs angle of magnetic field with plane of layers for $TaS_1Se_1$ and $NbSe_2$. Theoretical curves for $1/\sin^2\theta$ and for $\epsilon^2 = 0.022$ are shown for comparison.

$\xi_\parallel/\xi_\perp = 6.9$ and $m_\perp \approx 46 m_\parallel$. The results on all of the pure-tantalum compounds therefore show approximately the same anisotropy in coherence-length and effective-mass ratio within the accuracy of the present model. The triangles in Fig. 11 represent the data on pure $NbSe_2$ for comparison and clearly show the smaller anisotropy exhibited by this compound.

As previously shown in the experimental data of Fig. 8, intercalation of $TaS_1Se_1$ did not appreciably change the critical-field ratios and consequently the generalized effective-mass ratio is essentially unchanged. However, in the intercalated material the resistive transitions at low angles were spread over much larger field ranges indicating that appreciable layer separation had occurred. The layer separation would be expected to increase the band mass perpendicular to the layers due to less overlap of the wave functions, and the fact that no change in effective-mass ratio is observed is not readily explainable. Incomplete or nonuniform intercalation may be the explanation since the behavior may be very sensitive to the presence of filaments of pure material along the $c$-axis direction. The electron-phonon interaction is obviously influenced by the intercalation as evidenced by the change in $T_c$, but no information is available on its role in the basic anisotropic behavior.

Further information on the relative anisotropies in electron band mass and electron-phonon interaction will have to await further experiments such as Fermi-surface measurements and independent measurements of the superconducting anisotropy. Fermi-surface determination by such methods as cyclotron resonance or de Haas–van Alphen effect would be useful, but may be complicated by the fact that the cyclotron mass is enhanced by the factor[14] $(1+\lambda)$ and this enhancement factor itself will be anisotropic. Direct measurements of the superconducting energy gap such as tunneling in layer structures would also be useful for obtaining a more complete picture of the anisotropy.

## V. BAND STRUCTURE AND FERMI SURFACE IN $NbSe_2$ AND $TaS_2$

A number of papers[15] have considered the possible band structures of the transition-metal dichalcogenides. Huisman *et al.*[16] have considered those with trigonal-prismatic coordination in terms of crystal field and simple molecular-orbital calculations. The electronic properties will depend mainly on the ligand-field splitting of the metal $d$ orbitals and the molecular-orbital calculations indicate that the nondegenerate $a_1'^*$ level has the lowest energy of the $d$ levels in trigonal-prismatic coordination. In the Nb and Ta dichalcogenides the atoms have a $d^1$ configuration and this leads to a partially filled narrow band arising from the $a_1'^*$ level as shown in Fig. 12. Additional electronic

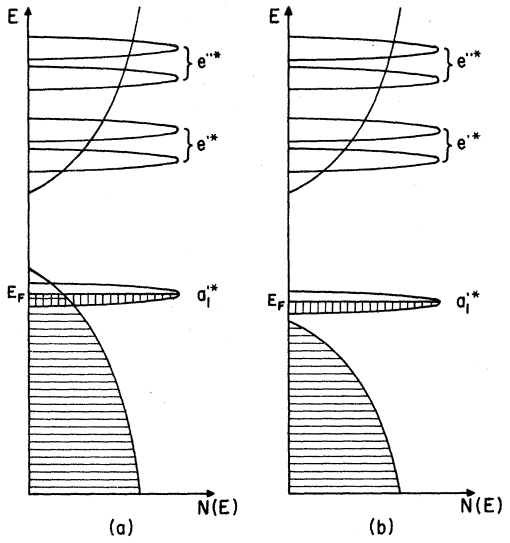


FIG. 12. Possible band structures for $TaS_2$ and $NbSe_2$ [after Huisman *et al.* (Ref. 16)].

states, derived from outer $s$ and $p$ orbitals of metal and ligand atoms, give rise to a valence band and this is also indicated in Fig. 12. Thompson *et al.*[4] have concluded that in $2H$-$TaS_2$ at helium temperatures the heavy-electron $d$ band does not overlap the light-hole valence band as shown in Fig. 12(b), but that at room temperature the bands do overlap as shown in Fig. 12(a). The case of $NbSe_2$ is very similar except that the band-overlap question is not as clear. Both compounds show phase transitions below 100 and 40 °K with a change of sign in the Hall resistivity at 56 and 40 °K for $TaS_2$ and $NbSe_2$, respectively. Marezio *et al.*[17] have connected this behavior with a structural transformation, and Ehrenfreund *et al.*[18] suggest that an associated conduction-electron redistribution occurs.

In the case of $NbSe_2$, Bromley[19] has recently considered the possible effects of interlayer bonding and this can cause a splitting of the two-dimensional energy levels considered in all of the previous calculations. The Fermi surface of the $2H$-$NbSe_2$ could then have additional pieces arising from this splitting and these could be partially holelike due to cutting of the prism faces of the hexagonal zone by the Fermi surface. In any event, all of the models would suggest a substantial contact of the Fermi surface with the hexagonal faces of the zone, and therefore the Fermi surface would be of the undulating cylinder type and this would lead to a generally anisotropic band mass.

Geilikman and Kresin[20] have considered the anisotropy of the energy gap in superconductors for both an elliptical and cylindrical model of the Fermi surface and the anisotropy in $\Delta(k)$ derived by them for the cylindrical model depends on the ratio $k_z(\max)/k_\perp$, where $k_\perp$ is the radius of the cylinder. However, the expressions would require considerable evaluation in order to arrive at any quantitative conclusions applicable to the present experiment. At present the correlation between the energy-gap anisotropy, the suggested Fermi-surface anisotropy, and the associated effective-mass anisotropy is difficult to sort out without additional experiments. The generalized effective-mass anisotropy measured in the critical-field experiments contains quite a bit of information on the anisotropic electronic properties, but too many assumptions are required to separate the various terms contributing to the anisotropy. Some model of the anisotropic electron-phonon interaction would be useful as well as direct measurements of the Fermi-surface anisotropy.

## VI. SUMMARY AND CONCLUSIONS

Measurements of the critical-field anisotropy in the layer compounds $NbSe_2$, $TaS_2$, $TaS_2$-(pyridine), $TaS_1Se_1$, $TaS_1Se_1$-(pyridine), $TaS_{0.8}S_{1.2}$, and $TaS_{1.2}Se_{0.8}$ have been compared in order to obtain estimates of the anisotropy of the coherence length in these materials. The anisotropy varies by a factor of 10 between the various compounds and as expected is largest for the more perfectly intercalated specimens of $TaS_2$. This behavior, as well as the magnetoresistance anisotropy in the normal state, suggests that the $TaS_2$-(pyridine) crystals are approaching a behavior characteristic of a two-dimensional conductor. The intercalated crystals also show very broad resistance transitions for fields applied at angles less than 10° from the orientation parallel to the layers and for certain orientations strong resistance maxima and minima are observed in the transition region. The transition behavior suggests that an enhanced flux flow may play a role in the intercalated material, but no satisfactory model has as yet been worked out.

The measured critical-field anisotropy gave an estimate for the coherence-length ratio $\xi_\parallel/\xi_\perp$ of approximately 7 for all of the pure tantalum compounds measured, as compared to the ratio 3.3 previously measured for pure $NbSe_2$. Intercalation of $TaS_2$ with pyridine increased the ratio $\xi_\parallel/\xi_\perp$ to approximately 20. In the case of the tantalum compounds with both S and Se present, intercalation did not appreciably change the anisotropy. This is most likely to be connected with imperfect intercalation although a change in the anisotropy of the electron-phonon interaction may also play some role. Estimates of the effective-mass ratios based on an elliptical model were $m_\perp \approx 46 m_\parallel$ for the pure tantalum compounds and $m_\perp \approx 400 m_\parallel$ for $TaS_2$-(pyridine), while the previous estimate for pure $NbSe_2$ was $m_\perp \approx 11 m_\parallel$.

ACKNOWLEDGMENTS

The authors would like to acknowledge Professor D. Sellmyer for contributions to parts of this work. Professor Leo Falicov and Rajendra Bhandari have made valuable contributions to interpretation of the data and Philipp Sommer and Werner Frewer have constructed parts of the apparatus.

*Work supported by Office of Naval Research and U. S. Atomic Energy Commission.

†Work above 80 kOe was performed while the authors were Guest Scientists at the Francis Bitter National Magnet Laboratory, which is supported at MIT by the National Science Foundation.

[1]D. J. Beerntsen, G. A. Spiering, and C. H. Armitage, IEEE Trans. Aerosp. **2,** 816 (1964).

[2]G. A. Spiering, E. Revolinsky, and D. J. Beerntsen, J. Phys. Chem. Solids **27,** 535 (1966).

[3]E. A. Antonova, S. A. Medvedev, and I. Yu. Shebalin, Zh. Eksp. Teor. Fiz. **57,** 329 (1969) [Sov. Phys.-JETP **30,** 181 (1970)].

[4]A. H. Thompson, R. F. Gamble, and R. F. Koehler, Jr., Phys. Rev. B **5,** 2811 (1972).

[5]R. C. Morris, R. V. Coleman, and Rajendra Bhandari, Phys. Rev. B **5,** 895 (1972).

[6]M. H. Van Maaren and G. M. Schaeffer, Phys. Lett. **20,** 131 (1966); R. Kershaw, M. Vlasse, and A. Wold, Inorg. Chem. **6,** 1599 (1967).

[7]F. R. Gamble, F. J. DiSalvo, R. A. Klemm, and T. H. Geballe, Science **168,** 568 (1970).

[8]Y. B. Kim and M. J. Stephin, in *Superconductivy,* edited by R. D. Parks (Marcel Dekker, New York, 1969), p. 1120.

[9]S. Foner, E. J. McNiff, Jr., A. H. Thompson, F. R. Gamble, T. H. Geballe, and F. J. DiSalvo, Bull. Am. Phys. Soc. **17,** 289 (1972).

[10]Alexander L. Fetter and Pierre C. Hohenberg, in Ref. 8, p. 860.

[11]W. E. Lawrence and S. Doniach, in *Proceedings of International Conference on Low Temperature Physics, 1970* (Academic Press of Japan, Tokyo, 1970), Vol. 12, p. 361.

[12]R. Bachmann, H. C. Kirsch, and T. H. Geballe, Solid State Commun. **9,** 57 (1971).

[13]M. H. Van Maaren and H. B. Harland, Phys. Lett. A**29,** 571 (1969).

[14]W. L. McMillan, Phys. Rev. **167,** 331 (1968).

[15]See, for example, J. A. Wilson and A. D. Yoffe, Adv. Phys. **18,** 193 (1969); R. B. Murray, R. A. Bromley, and A. D. Yoffe, J. Phys. C **5,** 746 (1972); R. A. Bromley, R. B. Murray, and A. D. Yoffe, J. Phys. C **5,** 759 (1972).

[16]R. Huisman, R. DeJonge, C. Hass, and F. Jellinek, J. Solid State Chem. **3,** 56 (1971).

[17]M. Marezio, P. D. Dernier, A. Menth, and G. W. Hull, Jr., J. Solid State Chem. **4,** 425 (1972).

[18]E. Ehrenfreund, A. C. Gossard, F. R. Gamble, and T. H. Geballe, J. Appl. Phys. **42,** 1491 (1971).

[19]R. A. Bromley, Phys. Rev. Lett. **29,** 357 (1972).

[20]B. T. Geilikman and V. Z. Kresin, Fiz. Tverd. Tela **5,** 3549 (1963) [Sov. Phys.-Solid State **5,** 2605 (1964)].

PHYSICAL REVIEW B VOLUME 7, NUMBER 3 1 FEBRUARY 1973

# Magnetic Field Dependence of the Surface Resistance of Pure and Impure Superconducting Aluminum at Photon Energies near the Energy Gap*

W. V. Budzinski,† M. P. Garfunkel, and R. W. Markley‡
*University of Pittsburgh, Pittsburgh, Pennsylvania* 15213

(Received 17 July 1972)

The magnetic field dependence of the microwave absorptivity of superconducting aluminum single crystals has been determined in the frequency range 15–100 GHz, covering the spectrum near the superconducting energy gap. Measurements were made on samples of varying purity, from the purest available alumimum to aluminum doped with 3-at.% silver. In the pure case, the energy of the absorption edge was found to shift with static magnetic field by an amount of the order $pv$, where $p$ is the Fermi momentum and $v$ is the drift velocity associated with the Meissner current. The addition of impurities was found to reduce the shift in the absorption edge as expected. Furthermore, the impurities coupled with the static field to induce an unexpected effect, namely, an absorption peak near the energy of the zero-field absorption edge. The amplitude of the absorption peak was found to increase monotonically with both magnetic field and with concentration of the silver impurity. A suggestion is made that impurities and magnetic field induce a change in the BCS coherence factors (from case II to case I) which, in turn, is responsible for the absorption peak.

## I. INTRODUCTION

For some years we have been making measurements of the effect of a static magnetic field on the microwave absorptivity of superconducting aluminum at photon energies $\hbar\omega$ near the energy gap $2\Delta$. Some of our early results have already appeared in abbreviated form[1–5] and there have been several papers dealing with the theory.[5–7] It is the purpose of this paper to present a complete account of our experiments.

The study of the microwave absorption of superconductors in a static magnetic field has consistently caused difficulties in fitting the existing theo-